



# Similarity between structural and proxy estimates of brain connectivity

Aldana Lizarraga<sup>1</sup>, Isabelle Ripp<sup>1</sup> , Arianna Sala<sup>1,2</sup>, Kuangyu Shi<sup>3</sup>, Marco Düring<sup>4</sup>, Kathrin Koch<sup>5</sup> and Igor Yakushev<sup>1</sup>

## Abstract

Functional magnetic resonance and diffusion weighted imaging have so far made a major contribution to delineation of the brain connectome at the macroscale. While functional connectivity (FC) was shown to be related to structural connectivity (SC) to a certain degree, their spatial overlap is unknown. Even less clear are relations of SC with estimates of connectivity from inter-subject covariance of regional F18-fluorodeoxyglucose uptake ( $FDG_{cov}$ ) and grey matter volume ( $GMV_{cov}$ ). Here, we asked to what extent SC underlies three proxy estimates of brain connectivity: FC,  $FDG_{cov}$  and  $GMV_{cov}$ . Simultaneous PET/MR acquisitions were performed in 56 healthy middle-aged individuals. Similarity between four networks was assessed using Spearman correlation and convergence ratio (CR), a measure of spatial overlap. Spearman correlation coefficient was 0.27 for SC-FC, 0.40 for SC- $FDG_{cov}$  and 0.15 for SC- $GMV_{cov}$ . Mean CRs were 51% for SC-FC, 48% for SC- $FDG_{cov}$ , and 37% for SC- $GMV_{cov}$ . These results proved to be reproducible and robust against image processing steps. In sum, we found a relevant similarity of SC with FC and  $FDG_{cov}$ , while  $GMV_{cov}$  consistently showed the weakest similarity. These findings indicate that white matter tracts underlie  $FDG_{cov}$  to a similar degree as FC, supporting  $FDG_{cov}$  as estimate of functional brain connectivity.

## Keywords

DWI, fMRI, functional connectivity, molecular connectivity, multimodal imaging

Received 15 April 2023; Revised 1 August 2023; Accepted 18 August 2023

## Introduction

Diffusion weighted imaging (DWI) and functional magnetic resonance imaging (fMRI) have so far made a major contribution to delineation of the human brain connectome at the macroscale. Structural connectivity (SC) refers to a physical link between two regions that is inferred from 3D reconstructions of white matter (WM) fiber tracts from DWI data.<sup>1</sup> In a broad sense, functional connectivity (FC) is defined as ‘statistical dependencies among remote neurophysiological events.’<sup>2</sup> The most common technique to capture FC is fMRI, where neural activity is inferred from variations in blood oxygen level dependent (BOLD) signals over time.<sup>3</sup> To avoid misunderstandings, we reserve the term “FC” for fMRI-derived connectivity estimates thereafter. A number of studies found that estimates of SC and FC were positively correlated, albeit to a variable degree.<sup>4–9</sup> Of note, FC was also observed between regions where there was little or no SC,<sup>5,10</sup> supporting the view that FC is partially mediated by

indirect pathways. However, data on spatial overlap between SC and FC at the whole brain level are still missing.

Information on brain connectivity has also been inferred from structural magnetic resonance imaging

<sup>1</sup>Department of Nuclear Medicine, School of Medicine, Klinikum Rechts der Isar, Technical University of Munich, Munich, Germany

<sup>2</sup>Coma Science Group, GIGA Consciousness, University of Liege; Centre du Cerveau<sup>2</sup>, University Hospital of Liege, Avenue de L'Hôpital 1, Liege, Belgium

<sup>3</sup>Department of Nuclear Medicine, University Hospital Bern, Bern, Switzerland

<sup>4</sup>Medical Image Analysis Center (MIAC AG) and Qbig, Department of Biomedical Engineering, University of Basel, Basel, Switzerland

<sup>5</sup>Department of Neuroradiology, School of Medicine, Klinikum Rechts der Isar, Technical University of Munich, Munich, Germany

## Corresponding author:

Igor Yakushev, Dept. of Nuclear Medicine, Technical University of Munich, Ismaninger Str. 22, 81675 Munich, Germany.

Email: igor.yakushev@tum.de

(sMRI) data, such as T1-weighted images.<sup>11</sup> In contrast to time series of fMRI, sMRI data are available for analyses as one single image per subject. Thus, sMRI-based connectivity estimation relies on identification of inter-subject covariance patterns at a group level. This approach has produced valuable insights into brain connectivity both in healthy<sup>12,13</sup> and pathological conditions, such as Alzheimer's disease<sup>14</sup> and schizophrenia.<sup>15</sup> The covariance patterns have been interpreted as a result of mutual trophic influences mediated by axonal connections or experience-related neural plasticity.<sup>12</sup> A number of studies found a significant similarity of this connectivity estimate with SC,<sup>6,16</sup> as well as with FC.<sup>6,17,18</sup>

There is increasing evidence that molecular imaging can effectively contribute to the study of the brain connectome.<sup>19</sup> Similar to sMRI, PET-based connectivity estimation is commonly performed at a group level. This approach has been successfully applied to PET measures of glucose metabolism,<sup>20–22</sup> neurotransmission,<sup>23,24</sup> and pathological protein aggregations.<sup>25–27</sup> The most popular approach has been PET with 18 F-Fluorodesoxyglucose (FDG), sometimes referred to in the literature as metabolic connectivity.<sup>28</sup> Instead, we now propose the term  $FDG_{cov}$ , inter-subject covariance of regional FDG-PET measures, to discriminate it from connectivity estimates from functional PET.<sup>29</sup>  $FDG_{cov}$  was found to provide valuable insights into healthy brain function<sup>30,31</sup> as well as into pathophysiology and diagnosis of numerous neuropsychiatric disorders.<sup>22,32–36</sup> So far, only one study has mapped  $FDG_{cov}$  to SC.<sup>37</sup> Specifically, our group found that around a half of  $FDG_{cov}$  connections had a structural substrate at the whole brain level. Neither FC nor covariance in gray matter (GM) characteristics were analyzed in our previous study. Furthermore, the cohort included both patients and healthy subjects, and the analysis of similarity was limited to a spatial overlap.<sup>37</sup>

So far, just two studies have investigated the similarity between connectivity estimates derived from at least three imaging techniques.<sup>6,18</sup> Di and colleagues reported low correlation between FC, covariance in GM volume ( $GMV_{cov}$ ), and  $FDG_{cov}$ , as well as a limited proportion of overlapping connections. SC was not quantified by the authors. Further, that work included data from multiple sites, acquired with varying imaging protocols and with PET and MRI acquisitions lying up to 4 years apart. Another study compared four estimates of connectivity in human and primate data: FC, covariance in cortical thickness, SC from tract-tracing (in monkeys), and SC from DWI tractography.<sup>6</sup> They found a poor general agreement, with DWI-SC and FC having the strongest similarity. That study included no PET data.

In the present work we asked to what degree SC may underlie  $FDG_{cov}$  in comparison with more established MR-based estimates of brain connectivity, FC and  $GMV_{cov}$ . Herewith, we explicitly treat SC as reference, because it is indicative of actual anatomical connectivity, reproducible,<sup>38</sup> and available at a single subject level. In contrast, the estimates FC,  $FDG_{cov}$ ,  $GMV_{cov}$  are based on statistical dependencies between regional signals;<sup>2</sup> we refer to them as *proxy* estimates of brain connectivity thereafter. To address these questions, DWI, fMRI, sMRI, and FDG-PET data were acquired simultaneously in a large group of healthy individuals on a hybrid PET/MR scanner. As both FDG uptake and BOLD signal index neural activity, we hypothesized that SC- $FDG_{cov}$  would be closer to SC-FC rather than to SC- $GMV_{cov}$ . This is far from obvious, since unlike FC,  $FDG_{cov}$  and  $GMV_{cov}$  are quantified from inter-subject variability.<sup>11</sup>

## Materials and methods

### Participants

By means of advertisements in internet and on hospital bulletin boards we recruited healthy, right-handed, German-speaking individuals at the age of 50 to 65 years old. Exclusion criteria were self-reported or objective (test battery) cognitive impairment, history of a neurological or psychiatric disorder, contraindications for MRI, and relevant anomalies on structural MRI images, including cerebrovascular disease. Data of 8 subjects were excluded for the following reasons: excessive motion, i.e., more than 3 mm or 3° maximum displacements during scanning ( $n=2$ ), large falx ossifications ( $n=1$ ), wrong phase encoding direction in DWI ( $n=4$ ), and incomplete data set ( $n=1$ ). Thus, the data of 56 individuals (25 females, mean  $\pm$  SD age:  $56 \pm 4$  years) were available for the present study. The study was performed in accordance with the ethical standards as laid down in the 1964 Declaration of Helsinki. The study was approved by the Federal Office for Radiation Protection and the Ethics Review Board of the University Hospital Klinikum rechts der Isar, Technical University of Munich (project number 399/13). All participants provided written, informed consent.

### Image acquisition

The participants were scanned in a 3T PET/MR Siemens Biograph mMR scanner with a vendor-supplied 16-channel head coil. They were instructed to fast for six hours prior to the scan session. After the intravenous injection of on average  $102 \pm 5$  (SD) MBq of 18 F-FDG, the participants stayed

comfortably in a quiet, dimly lit room, with closed eyes. Reconstructed PET images (30–60 min post-injection) had a voxel size of  $1.04 \times 1.04 \times 2.03 \text{ mm}^3$ . Anatomical T1-weighted images were acquired with a magnetization-prepared rapid gradient-echo (MP-RAGE) sequence with a voxel size of  $1.0 \times 1.0 \times 1.0 \text{ mm}^3$ . DWI was performed using a single-shot EPI sequence of voxel size  $2 \times 2 \times 2 \text{ mm}^3$ , with 30 diffusion directions with  $b = 800 \text{ s/mm}^2$  and one volume with  $b = 0 \text{ s/mm}^2$ . For the fMRI acquisition, which lasted 8 min, participants were instructed to stay awake, close their eyes and think of nothing in particular. 212 volumes were acquired using a Prospective Acquisition Correction EPI sequence with voxel size of  $3.0 \times 3.0 \times 3.0 \text{ mm}^3$ . An ultra-short echo time sequence was acquired for attenuation correction of the PET data. A dual echo gradient echo sequence was acquired to correct the DWI images for susceptibility induced distortions. Details of the PET and MR acquisitions are given in the supplementary material to our recent article.<sup>39</sup>

### Grey matter parcellation

Estimation of connectivity indices from four imaging techniques required us to make a number of methodological decisions. One of the major challenges was the choice of a parcellation scheme from a vast variety of available brain atlases. Finally, we decided to use the Automated Anatomical Labeling 2 (AAL2) atlas<sup>40</sup> for the following reasons: a) it includes cortex, cerebellum, and subcortical regions, b) it has a lower proportion of small regions, an important advantage in light of potential partial volume effects in PET data, c) it is more robust than other atlases against non-linear registrations (data not shown), d) it has a simple nomenclature, e) it is the most widely used atlas, making a comparison with the literature more straightforward. Since AAL2 regions are defined in a way that their borders extend beyond GM, we sampled only GM part of those regions (see below). Another important methodological issue was a registration approach. We decided to keep the images in the native (individual) space and transform the atlas from the MNI space to the individual space, in order to reduce data manipulation and have a better visual control over accuracy of registration. Thus, the AAL2 parcellation was non-linearly transformed from the MNI152 T1 space to the individual T1 space using Advanced Normalization Tools (ANTs).<sup>41</sup> Afterwards, T1 images were segmented using SPM12 (<https://www.fil.ion.ucl.ac.uk/spm/software/spm12/>). GM probability maps were then binarized at a probability of 0.5, followed by parcellation. Certain regions of the original parcellation were combined or removed in order to minimize the number of small regions (volume  $< 512 \text{ mm}^3$ , i.e.  $2 \times \text{FWHM}$  in all

directions). Finally, we obtained a parcellation of 106 regions. The list of regions and further details are given in the Supplementary Material.

### Structural connectivity network

We obtained SC networks from DWI data using tools of the FMRIB Software Library (FSL). After visual inspection of the images by means of FSLeaves, we estimated the field map with *fsl\_prepare\_fieldmap* and corrected for susceptibility induced distortions, eddy currents, inter-volume movement, and signal dropout using *eddy*.<sup>42</sup> Then, we extracted brain tissue with BET<sup>43</sup> and fit the Ball and Sticks diffusion model with  $N=2$  using BedpostX.<sup>44</sup> Afterwards, we performed whole brain probabilistic tractography using a WM seeding approach with ProbtrackX. To this end, 0.5 thresholded masks of GM, WM, and CSF were used as target, seed and exclusion masks, respectively. To allow transformation of the masks from the T1 space to the DWI space, in which the tractography was performed, a linear transformation was provided to ProbtrackX. As an estimate of SC we used the number of streamlines connecting two GM regions and normalized them by the surface area of those regions in the WM-GM interface to compensate for surface-driven effects on streamline counts.<sup>45,46</sup> In order to construct a group SC network, we resampled the connection weights, i.e. strength, of each subject to Gaussian distribution<sup>5,47</sup> and calculated an average across subjects. Following multiple studies, we applied a proportional threshold to retain connections present in more than 75% of subjects.<sup>48–50</sup> This resulted in a network density of 34%.

### Functional connectivity network

FC was inferred from fMRI data. The diagnostic tool *tsdiffana* was utilized in MATLAB v2020a software (The MathWorks Inc., Natick, Massachusetts, USA) to detect corrupted frames that might not be noticed visually. After removal of the first three volumes of the BOLD series, the images were corrected for slice timing and realigned to the volume acquired temporally in the middle using SPM12. We created WM and CSF masks applying a threshold of 0.99 to the probability maps from the T1 segmentation. Those masks, as well as the GM parcellation, were linearly transformed from the T1 space to the BOLD space using the FSL registration tool FLIRT with a nearest neighbor interpolation.<sup>51</sup> After that, we regressed the WM and CSF signal components using *fsl\_glm*. Motion was not regressed out, as this may reduce reliability.<sup>52</sup> Instead, we checked that none of the included subjects showed an excessive motion ( $> 3 \text{ mm}$  or  $> 3^\circ$ ). A temporal band-pass filter

(0.009–0.080 Hz) was applied to reduce non-BOLD high frequency signals due to heart rate and breathing and lower frequency signals due to scanner instability.<sup>4</sup> Next, we extracted the signal from each region and calculated the Pearson correlation between each pair of regions. In order to build a group FC network, we applied a Fisher z-transformation to the correlation coefficients, averaged them across subjects and transformed them back to Pearson correlation coefficients.<sup>18</sup>

### Covariance networks

A group network of  $FDG_{cov}$  was estimated from FDG-PET images. After a linear registration of PET images to the individual T1 space with SPM, FDG uptake was extracted from each region and normalized by mean GM uptake.<sup>53</sup> Finally, Pearson correlations were calculated between each pair of regions across subjects.

To keep the cerebellum and subcortical structures in the analyses, we decided to use GM volume rather than GM thickness as morphological feature. GM volume (GMV) was calculated for each region as a sum of GM probabilities multiplied by the voxel size. Afterwards, we regressed out the total GMV of each subject.<sup>54</sup> Finally, Pearson correlation of the residuals between pairs of regions was calculated across subjects to obtain a symmetric 106x106 matrix.

### Similarity between the networks

To assess similarity between the networks in terms of strength, we calculated Spearman correlations between connection weights of a network pair. This non-parametric test was chosen, as the connection weights were not normally distributed (Kolmogorov-Smirnov test). As the biological meaning of negative FC as well as negative  $FDG_{cov}$  and  $GMV_{cov}$  is still under discussion,<sup>55</sup> we in addition re-calculated the correlations for positive connections weights only.<sup>18,56</sup>

To assess similarity between the networks in terms of spatial distribution, we calculated convergence ratio (CR), the number of common connections divided by the average of the connections in a network pair. This index is equivalent to Dice similarity coefficient. To this end, the networks need to be binarized via thresholding. Common approaches are 1) removal of connections below a minimum connection weight,<sup>57</sup> 2) removal of connections below a desired density/sparsity,<sup>58</sup> where the sparsity is defined as the number of null elements in its matrix divided by the total number of elements,<sup>50</sup> and 3) removal of connections above certain  $p$ -values of correlation coefficients.<sup>23,31</sup> While the approaches 1) and 3) produce networks with a different number of connections, 2) produces networks with the same number of connections but a different minimum weight. As the

spatial overlap between binary networks is affected by their sparsity, but independent of the connection weight, we decided to use the approach 2). Thus, CR between all network pairs was calculated at a sparsity range of 65.8% to 80%. The lower limit was imposed by the sparsity of the group SC network, which was 65.8% after the proportional thresholding step. The upper limit ensures that all networks are connected.<sup>16</sup> In graph theory, a network is connected, if one can go from a region A to a region B by following a path (link succession). Further, we computed CR expected by chance as described in the Supplementary Material.

As secondary analyses, we calculated similarity between the proxy estimates of brain connectivity only. Herewith, all possible connections, i.e., irrespective of SC, were considered. We note, however, that this comparison should be treated *with caution*, as in the absence of a reference standard, it is not clear which connections are true and which are artifactual.

### Robustness analyses

To assess robustness of our results, we repeated the analyses under different conditions, namely:

- a. Test-retest reproducibility, i.e., we analyzed imaging data acquired under the same conditions approximately 8 weeks later.<sup>39</sup>
- b. Omitting Gaussian resampling of SC, i.e., each element of the group SC matrix was calculated as average of normalized streamline counts across subjects.
- c. Omitting SC thresholding, i.e., no threshold was applied to the group SC matrix.
- d. Applying a more liberal proportional threshold of 50% to the SC matrix.
- e. Regressing out a distance between the regions. Since brain networks are spatially embedded, distance between regions might be a confound when estimating similarity between networks.<sup>7</sup> To take that into account, we calculated Euclidean distance between ROI centroids in the native space of each subject, followed by a linear regression of mean distances across subjects from the weight distribution of SC and proxy estimates of brain connectivity. Resultant residuals were used to recalculate CRs. In addition, partial Spearman correlations between connection weights were calculated using distance as covariate.
- f. Limiting the analysis to the cerebral cortex. To this end, vermis, cerebellum, and subcortical structures were excluded from the analysis, resulting in a parcellation of 80 cortical regions.

## Results

Figure 1 presents the adjacency matrices for each brain connectivity estimate, where each entry indicates the connection weight, i.e., strength of a link between regions. The SC matrix had a sparsity of 65.8%; no region was disconnected (Figure 1a). Unthresholded SC matrix is shown in Supplementary Figure 1.

Figure 2 shows histograms of connection weights. The connection weight distributions for all networks was unimodal, with a percentage of negative weights equal to 26% for FC, 52% for  $FDG_{cov}$ , and 53% for  $GMV_{cov}$ . Histograms of connection weights corresponding to the unthresholded SC network are shown in Supplementary Figure 2.

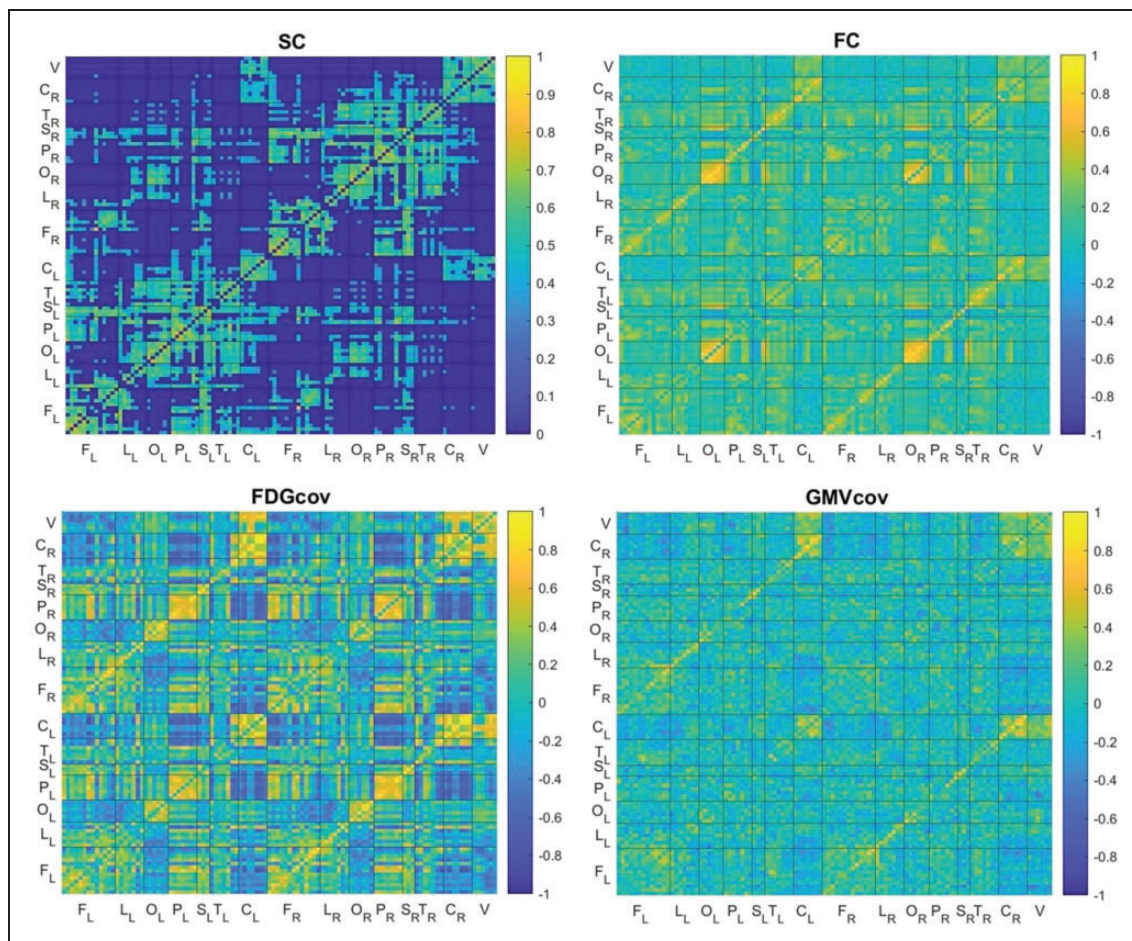
The scatterplots and Spearman correlation coefficients (SCC) between SC and the proxy estimates are shown in Figure 3. All SCC were positive and statistically significant ( $p$ 's < 0.001, Bonferroni corrected), decreasing in the order  $r=0.40$  for SC- $FDG_{cov}$ ,  $r=0.27$  for SC-FC, and  $r=0.16$  for SC- $GMV_{cov}$ .

The correlations for positive weights only are shown in Supplementary Figure 3. The coefficients decreased in the order  $r=0.31$  for SC-FC,  $r=0.26$  for SC- $FDG_{cov}$ , and  $r=0.18$  for SC- $GMV_{cov}$  ( $p$ 's < 0.001, Bonferroni corrected).

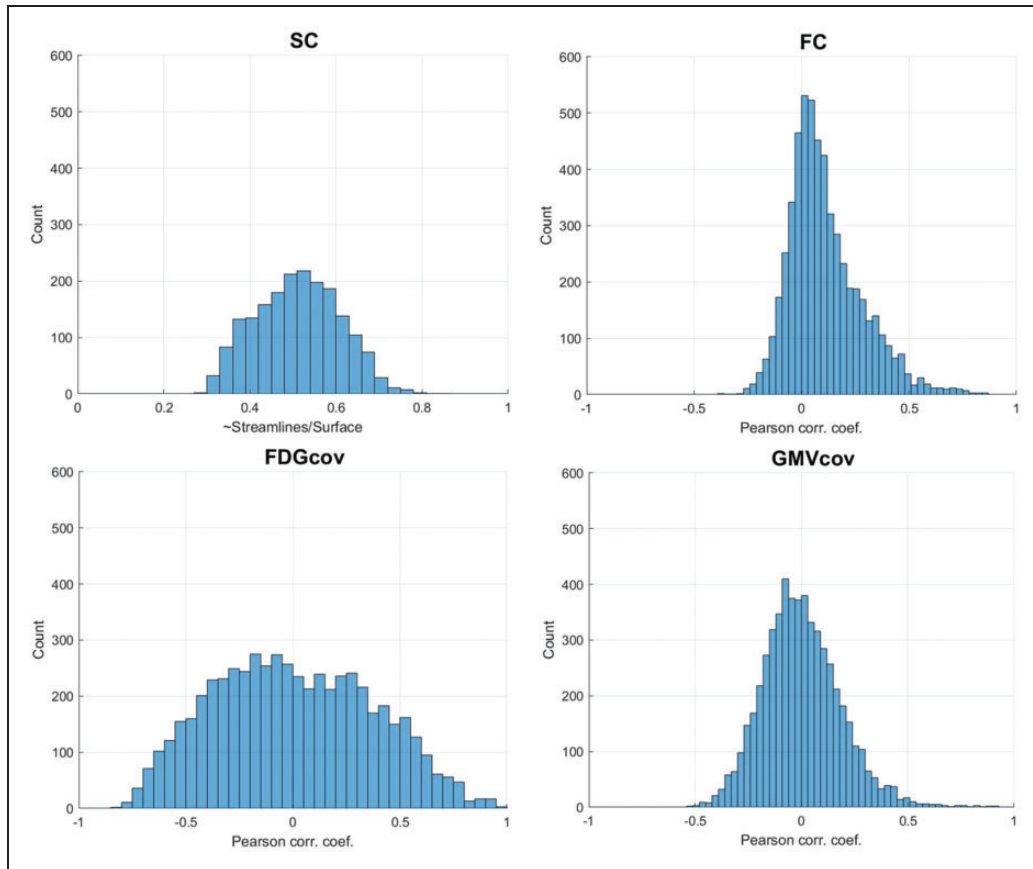
Spatial overlap as quantified by CR was substantially higher than that expected by chance for all networks (Figure 4). Mean CRs were 51% for SC-FC, 48% for SC- $FDG_{cov}$ , and 37% for SC- $GMV_{cov}$ .

Figure 5 presents an overlap between SC and the proxy estimates at 80% sparsity. Overall, it was stronger for intralobe connections and homotopic interhemispheric connections, especially in the cerebellum (hemispheres and vermis). In addition,  $FDG_{cov}$  and FC stronger overlapped with SC in the occipital and frontal lobes.

SCC between weights of the proxy estimates were  $r=0.30$  for FC- $FDG_{cov}$ ,  $r=0.25$  for FC- $GMV_{cov}$ , and  $r=0.22$  for  $FDG_{cov}$ - $GMV_{cov}$  (Supplementary Figure 4). CRs for the proxy estimates were 46% for



**Figure 1.** Group matrix for each connectivity estimate. The color bars indicate connection weights. The 106 regions were grouped into the following structures: frontal (F), limbic (L), occipital (O), parietal (P), subcortical (S), temporal (T), cerebellar hemispheres (C), and vermis (V). The subscript indicates the left (L) and right (R) hemisphere.



**Figure 2.** Distribution of edge/connection weights for each estimate.

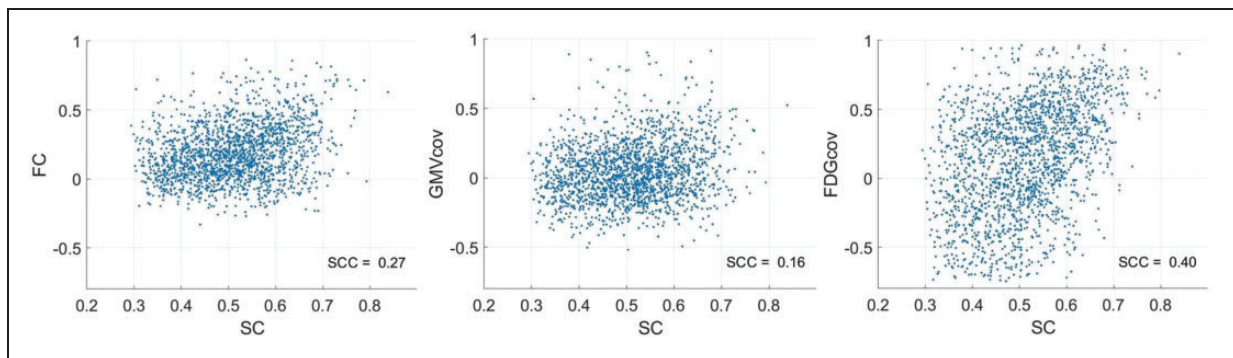


**Figure 3.** Scatter plots of connection weights and Spearman correlation coefficients for SC and the proxy estimates.

FDG<sub>cov</sub>-FC, 43% for GMV<sub>cov</sub>-FC, and 40% for FDG<sub>cov</sub>-GMV<sub>cov</sub> (Supplementary Figure 5).

Results of the robustness analyses are presented in Table 1. Overall, the measures of similarity did not change substantially. First, the entire analysis proved to be highly reproducible, including the limits of the sparsity interval (66.1–79.8%) (a). Omitting Gaussian resampling affected neither sparsity of the SC matrix nor the ranking of similarities between the networks (b). Omitting SC thresholding led to a denser SC

matrix with a sparsity of 13.3% (c). A resultant wider sparsity interval did not change significantly SCC, but increased systematically CRs, making them closer to CR by chance (c). Application of a more liberal proportional threshold of 50% to the SC matrix produced sparsity of 55%. Beside an expected increase in CRs, the similarity metrics showed the same behavior as before (d). Regressing out the distance between regions altered maximum sparsity, at which all networks are to be connected, from 80% to 64.7%. This precluded us

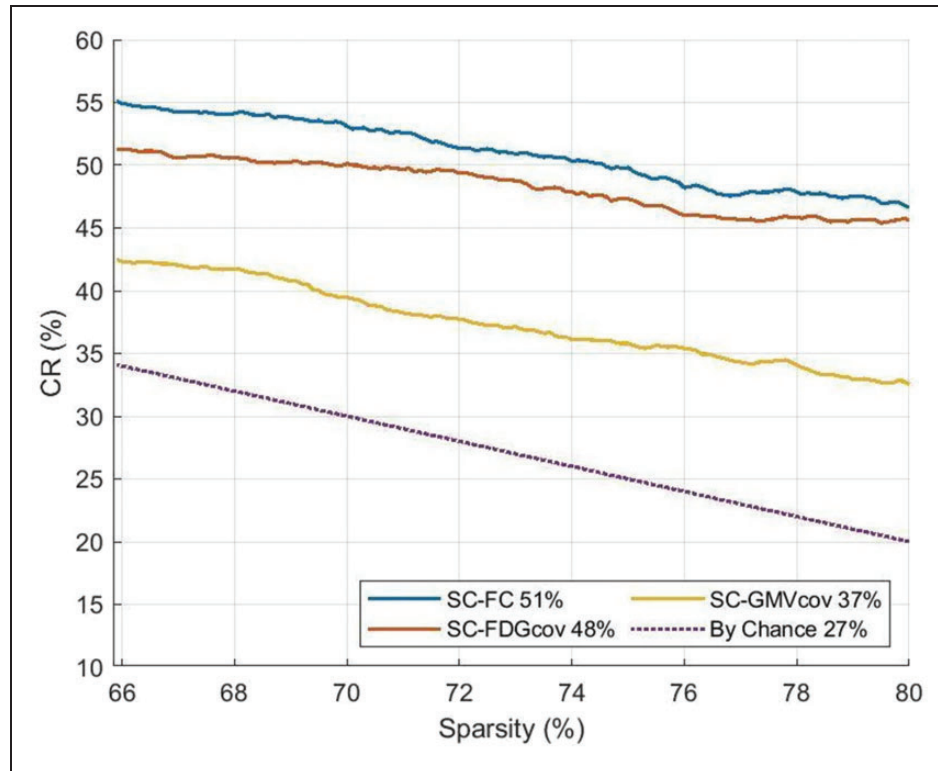


**Figure 4.** Convergence ratio (CR) between SC and proxy estimates as a function of sparsity level. The percentages indicate mean CRs over the sparsity range.

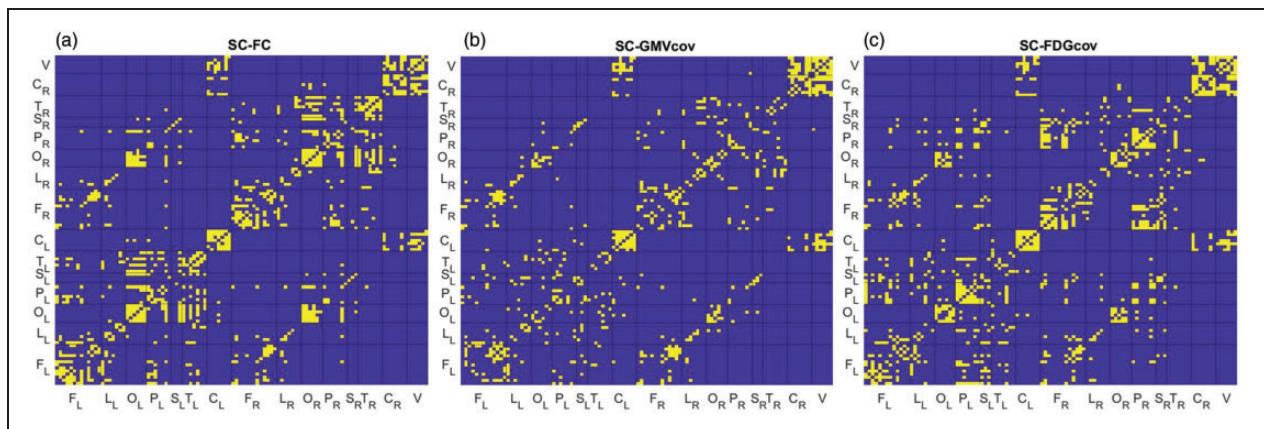


**Figure 5.** Overlap matrices between SC and proxy estimates as a function of sparsity level. Yellow elements indicate common connections after thresholding the networks at 80% sparsity.

from applying the connectedness criterion to set the upper limit of the sparsity range. Therefore, we kept the previous sparsity range (65.8–80.0%). As expected, both SCCs and CRs decreased when distance between regions was regressed out, but CR values were still well above those expected by chance (e). Finally, when the analyses were limited to the cortex (f), SCC and CR values remained similar. The measures of similarity

between the proxy estimates only did not change substantially, too (Supplementary Table 2).

## Discussion

In the present study, we examined similarity between SC and proxy estimates of brain connectivity FC,  $GMV_{cov}$ , and  $FDG_{cov}$ . All SCCs as index of similarity

**Table 1.** Robustness analyses.

	SCC						
	O	a)	b)	c)	d)	e)	f)
SC-FDG <sub>cov</sub>	0.40	0.41	0.42	0.32	0.38	0.26	0.38
SC-FC	0.27	0.24	0.27	0.31	0.29	0.11	0.34
SC-GMV <sub>cov</sub>	0.16	0.16	0.17	0.17	0.15	0.01	0.17
	CR						
SC-FDG <sub>cov</sub>	48	48	49	63	50	37	49
SC-FC	51	50	51	66	54	41	51
SC-GMV <sub>cov</sub>	37	37	37	59	42	29	36
CR by chance	27	27	27	53	32	27	30
Min sparsity	66	66	66	13	55	66	64
Max sparsity	80	80	80	80	80	80	77

Similarity metrics obtained under modified conditions relative to the original (O) ones: a) Test-retest reproducibility, b) Omitting the Gaussian resampling step of SC, c) Omitting the proportional threshold to SC matrix, d) Applying a 50% proportional threshold to the SC matrix, e) Regressing out distance from all connectivity estimates, f) limiting the analysis to the cerebral cortex. SCC: Spearman correlation coefficient; CR: mean convergence ratio computed over the corresponding sparsity range [min sparsity, max sparsity].

strength were significant, with a low to moderate degree. CRs as index of spatial similarity appeared to be higher than that by chance for all pairs of the estimates. The strongest similarity with SC was found for FC and FDG<sub>cov</sub>, while GMV<sub>cov</sub> consistently showed the weakest similarity. Of note, comprehensive additional analyses confirmed robustness of the findings.

Anatomical connections between brain regions are considered as structural core of brain connectivity.<sup>59</sup> To what degree does this core explain patterns of functional connectivity? By functional connectivity we explicitly mean here estimates of brain connectivity from measures of neural activity, such as fMRI and FDG-PET. The present results indicate that around a half of functional connections, both from fMRI and FDG-PET, are underlied by SC. While *spatial* similarity in terms of CR was slightly higher for fMRI, similarity in terms of SCC was higher for FDG<sub>cov</sub>. This is not implausible, because not identical connections were considered in the analyses. To calculate CR, 34% of the strongest connections in each network were considered. Hence, negative connections were excluded. In contrast, the Spearman correlations were restricted to structurally consistent connections, independently of their strength and sign. Thus, the relevance of a structural connection in terms of strength is more similar to that of FDG<sub>cov</sub> than FC, while the strongest FC spatially overlap somewhat better with structural connections than the strongest FDG<sub>cov</sub> connections. As expected, limiting the correlation analyses to positive connection weights produced the same order of similarity as CR, i.e. SC-FC > SC-FDG<sub>cov</sub>.

While FDG-PET has been increasingly utilized in the field of brain connectivity,<sup>19</sup> the meaning of

FDG<sub>cov</sub> and its relationship with the more established MRI-based estimates of brain connectivity has been unclear. The present study indicates that SC as estimated with DWI underlie FDG<sub>cov</sub> and FC to a similar degree. A relevant relationship between FC and FDG<sub>cov</sub> is further supported by our additional analyses of similarity between proxy estimates of connectivity, where FC and FDG<sub>cov</sub> showed the highest correlation and spatial overlap with each other. This result is intriguing, given important differences between the estimates, especially in respect to the targeted process, acquisition mode, and modeling approach.<sup>60</sup> We speculate that similarity might be even higher when indices of brain connectivity are derived from temporal correlations in dynamic FDG-PET data.<sup>29</sup> In contrast, similarity between GMV<sub>cov</sub> and FDG<sub>cov</sub> was lowest, even somewhat lower than that between GMV<sub>cov</sub> and FC. These observations strongly support FDG<sub>cov</sub> as index of functional connectivity rather than a sort of statistical artifact of inter-subject correlations.<sup>29,61</sup>

The first attempt to compare SC and FDG<sub>cov</sub> networks has been undertaken by our group very recently.<sup>37</sup> We found a spatial overlap of 55%, i.e. very similar value to that of the present work (48%). These similar results are rather surprising given a number of important differences between the studies in respect to study design and methods, e.g., population (patients and healthy subjects vs. healthy subjects only), atlases, number of regions (62 vs. 106), modeling approach of FDG<sub>cov</sub> (sparse inverse covariance estimation vs. correlation), method of tractography (deterministic vs. probabilistic), and index of SC (fractional anisotropy vs. normalized streamline counts). Despite the methodological differences the present work

supports our previous conclusion that around half of  $FDG_{cov}$  connections may have a structural substrate at the whole brain level.

Similarity between SC and FC has been extensively addressed in the literature, both in healthy and pathological conditions. Although the studies coincide in a positive association between these two estimates, the reported correlation values vary from weak to good,<sup>4-7,47,62</sup> likely due to methodological differences between the studies. The correlation coefficients in the present study are well within this range. We are not aware of any data on spatial overlap between SC and FC at the whole brain level. Here, we found a CR of 51%. In other words, roughly a half of functional connections have a structural substrate.

We explored for the first time GM covariance networks in combination with  $FDG_{cov}$ , SC, and FC in the same healthy subjects. So far, the biological mechanisms behind regional GM covariance have not been well understood. The most widespread hypotheses point at mutually trophic factors mediated by axonal connections,<sup>63</sup> activity-dependent processes,<sup>64</sup> common experience-related plasticity,<sup>63</sup> and genetics.<sup>65</sup> In the present study,  $GMV_{cov}$  showed the weakest similarity with the other estimates. Of note, our quantitative results closely resemble previously reported ones, despite a number of methodological differences. In particular, Gong et al. compared patterns of covariance of GM thickness with SC across the entire cerebral cortex.<sup>16</sup> For a similar sparsity level, they reported a CR of 33 to 37%, while we found a CR of 33 to 36%. Our results are furthermore well in line with those of Reid et al., who reported the weakest similarity for covariance of GM thickness with SC and FC.<sup>6</sup> Their SCCs were, however, higher, likely due to a better data quality and a lower resolution parcellation.<sup>5,6</sup> Further, Di and colleagues compared  $GMV_{cov}$ , FC, and  $FDG_{cov}$  networks through Spearman correlations and percentage of overlap.<sup>18</sup> Their SCCs were very close to ours and, alike, those for  $GMV_{cov}$  were the weakest. Like in the present study, similarity between the proxy estimates decreased in the following order  $FDG_{cov}$ -FC >  $FDG_{cov}$ - $GMV_{cov}$  > FC- $GMV_{cov}$  at the majority of sparsity levels. These observations support the conclusion above that  $FDG_{cov}$  as estimate of functional brain connectivity is closer to FC than to  $GMV_{cov}$ .

In this study, we decided to omit any streamline-length correction of SC weights. It is known that long-distance connections detected through tractography are fewer and weaker than short-distance connections.<sup>66</sup> To adjust for this, FSL's length correction multiplies the connectivity distribution by the expected length of pathways. However, this effect has also been observed in invasive tract tracing studies, such that the WM seeding approach applied here was suggested to

mitigate such a bias.<sup>67</sup> Nevertheless, we took into account the distance between regions in our robustness analyses. A systematic decrease in the similarity metrics suggests that spatial embedding might contribute to network similarity.<sup>4,5,7</sup>

A limitation of this study is a relatively low b-value as well as a low number of diffusion directions. Yet, while a higher b-value would increase the diffusion weighting of the images, it might also reduce their signal-to-noise ratio. Along these lines, increasing the number of directions would require a longer acquisition time of the DWI sequence, limiting practicability of multimodal imaging protocols as ours. Further, a required number of diffusion directions as well as an optimal b-value depend on the diffusion model to be applied.<sup>68</sup> Of note, the FSL *ball and sticks* model, as applied here, was shown to robustly detect crossing fibers in DWI data acquired with parameters close to ours.<sup>46</sup>

In summary, we found a relevant similarity of SC with FC and  $FDG_{cov}$ , while  $GMV_{cov}$  consistently showed the weakest similarity. These results indicate that SC underlies  $FDG_{cov}$ , inter-subject covariance of  $FDG$  uptake, to a similar degree as group FC, an established estimate of brain connectivity. This work underpins  $FDG_{cov}$  as index of *functional* brain connectivity. Future studies should compare properties of the different connectomes using e.g., graph theory metrics. Further, dependence of  $FDG_{cov}$  on intensity normalization should be explored.

### Funding

The author(s) disclosed receipt of the following financial support for the research, authorship, and/or publication of this article: This work was supported by the German Research Foundation (DFG), grants to I.Y. (grant number YA 373/3-1) and to K.K. (grant number KO 3744/8-1), and by the Federal Ministry of Education and Research Germany (BMBF), grant to I.Y. (grant number 031L0200B).

### Acknowledgements

We thank Brigitte Mackert, Sylvia Schachoff, and Claudia Meisinger for their valuable assistance in scheduling and conducting of PET/MR examinations.

### Data and code availability

Data and codes are available upon request.

### Declaration of conflicting interests

The author(s) declared no potential conflicts of interest with respect to the research, authorship, and/or publication of this article. IY received consultant or lecture fees from ABX-CRO, Blue Earth Diagnostics, and Piramal.

### Authors' contributions

AL, KS, MD, KK, IY contributed to the conception and design of the study. IR recruited the participants. AL, IR analyzed the neuroimaging data. AL, AS, IY wrote the manuscript. All authors contributed to the manuscript revision and approved the submitted version.

### Supplementary material

Supplemental material for this article is available online.

### ORCID iD

Isabelle Ripp  <https://orcid.org/0000-0002-3239-6711>

### References

- Smith R, Raffelt D, Tournier JD, et al. Quantitative streamlines tractography: methods and inter-subject normalisation. *Open Science Framework* 2020, <https://osf.io/c67kn> (accessed 9 March 2023).
- Friston KJ. Functional and effective connectivity: a review. *Brain Connect* 2011; 1: 13–36.
- Lowe MJ, Mock BJ and Sorenson JA. Functional connectivity in single and multislice echoplanar imaging using resting-state fluctuations. *NeuroImage* 1998; 7: 119–132.
- Skudlarski P, Jagannathan K, Calhoun VD, et al. Measuring brain connectivity: diffusion tensor imaging validates resting state temporal correlations. *NeuroImage* 2008; 43: 554–561.
- Honey CJ, Sporns O, Cammoun L, et al. Predicting human resting-state functional connectivity from structural connectivity. *Proc Natl Acad Sci U S A* 2009; 106: 2035–2040.
- Reid AT, Lewis J, Bezgin G, et al. A cross-modal, cross-species comparison of connectivity measures in the primate brain. *NeuroImage* 2016; 125: 311–331.
- Garcés P, Pereda E, Hernández-Tamames JA, et al. Multimodal description of whole brain connectivity: a comparison of resting state MEG, fMRI, and DWI. *Hum Brain Mapp* 2016; 37: 20–34.
- Zimmermann J, Griffiths J, Schirner M, et al. Subject specificity of the correlation between large-scale structural and functional connectivity. *Netw Neurosci* 2019; 3: 90–106.
- Messé A. Parcellation influence on the connectivity-based structure–function relationship in the human brain. *Hum Brain Mapp* 2020; 41: 1167–1180.
- Koch MA, Norris DG, Hund-Georgiadis M. and An Investigation of functional and anatomical connectivity using magnetic resonance imaging. *NeuroImage* 2002; 16: 241–250.
- Seghier ML and Price CJ. Interpreting and utilising inter-subject variability in brain function. *Trends Cogn Sci* 2018; 22: 517–530.
- Romero-Garcia R, Whitaker KJ, Váša F, NSPN Consortium, et al. Structural covariance networks are coupled to expression of genes enriched in supragranular layers of the human cortex. *NeuroImage* 2018; 171: 256–267.
- Seidlitz J, Váša F, Shinn M, NSPN Consortium, et al. Morphometric similarity networks detect microscale cortical organization and predict Inter-Individual cognitive variation. *Neuron* 2018; 97: 231–247.e7. Jan
- Montembeault M, Rouleau I, Provost JS, Alzheimer's Disease Neuroimaging Initiative, et al. Altered gray matter structural covariance networks in early stages of alzheimer's disease. *Cereb Cortex* 2016; 26: 2650–2662.
- Palaniyappan L, Hodgson O, Balain V, et al. Structural covariance and cortical reorganisation in schizophrenia: a MRI-based morphometric study. *Psychol Med* 2019; 49: 412–420.
- Gong G, He Y, Chen ZJ, et al. Convergence and divergence of thickness correlations with diffusion connections across the human cerebral cortex. *NeuroImage* 2012; 59: 1239–1248.
- Reid AT, Hoffstaedter F, Gong G, et al. A seed-based cross-modal comparison of brain connectivity measures. *Brain Struct Funct* 2017; 222: 1131–1151.
- Di X, Gohel S, Thielcke A, et al. Do all roads lead to Rome? A comparison of brain networks derived from inter-subject volumetric and metabolic covariance and moment-to-moment hemodynamic correlations in old individuals. *Brain Struct Funct* 2017; 222: 3833–3845.
- Sala A, Lizarraga A, Caminiti SP, et al. Brain connectomics: time for a molecular imaging perspective? *Trends Cogn Sci* 2023; 27: 353–366.
- Moeller JR, Strother SC, Sidtis JJ, et al. Scaled subprofile model: a statistical approach to the analysis of functional patterns in positron emission tomographic data. *J Cereb Blood Flow Metab* 1987; 7: 649–658.
- Sala A, Caminiti SP, Iaccarino L, et al. Vulnerability of multiple large-scale brain networks in dementia with Lewy bodies. *Hum Brain Mapp* 2019; 40: 4537–4550.
- Caminiti SP, Tettamanti M, Sala A, et al. Metabolic connectomics targeting brain pathology in dementia with Lewy bodies. *J Cereb Blood Flow Metab* 2017; 37: 1311–1325.
- Veronese M, Moro L, Arcolin M, et al. Covariance statistics and network analysis of brain PET imaging studies. *Sci Rep* 2019; 9: 2496.
- Vergier A, Horowitz T, Chawki MB, et al. From metabolic connectivity to molecular connectivity: application to dopaminergic pathways. *Eur J Nucl Med Mol Imaging* 2020; 47: 413–424.
- Hoenig MC, Bischof GN, Seemiller J, et al. Networks of tau distribution in Alzheimer's disease. *Brain* 2018; 141: 568–581.
- Ossenkopppe R, Iaccarino L, Schonhaut DR, et al. Tau covariance patterns in Alzheimer's disease patients match intrinsic connectivity networks in the healthy brain. *Neuroimage Clin* 2019; 23: 101848.
- Pereira JB, Ossenkopppe R, Palmqvist S, et al. Amyloid and tau accumulate across distinct spatial networks and are differentially associated with brain connectivity. *eLife* 2019; 8: e50830.
- Yakushev I, Drzezga A and Habeck C. Metabolic connectivity: methods and applications. *Curr Opin Neurol* 2017; 30: 677–685.

29. Jamadar SD, Ward PGD, Liang EX, et al. Metabolic and hemodynamic resting-state connectivity of the human brain: a high-temporal resolution simultaneous BOLD-fMRI and FDG-fPET multimodality study. *Cereb Cortex* 2021; 31: 2855–2867.
30. Zou N, Chetelat G, Baydogan MG, et al. Metabolic connectivity as index of verbal working memory. *J Cereb Blood Flow Metab* 2015; 35: 1122–1126.
31. Huang Q, Zhang J, Zhang T, et al. Age-associated reorganization of metabolic brain connectivity in Chinese children. *Eur J Nucl Med Mol Imaging* 2020; 47: 235–246.
32. Perani D, Farsad M, Ballarini T, et al. The impact of bilingualism on brain reserve and metabolic connectivity in Alzheimer's dementia. *Proc Natl Acad Sci U S A* 2017; 114: 1690–1695.
33. Titov D, Diehl-Schmid J, Shi K, et al. Metabolic connectivity for differential diagnosis of dementing disorders. *J Cereb Blood Flow Metab* 2017; 37: 252–262.
34. Pagani M, Giuliani A, Öberg J, et al. Progressive disintegration of brain networking from normal aging to Alzheimer disease: analysis of independent components of <sup>18</sup>F-FDG PET data. *J Nucl Med* 2017; 58: 1132–1139.
35. Verger A, Roman S, Chaudat RM, et al. Changes of metabolism and functional connectivity in late-onset deafness: evidence from cerebral 18F-FDG-PET. *Hear Res* 2017; 353: 8–16.
36. Shim HK, Lee HJ, Kim SE, et al. Alterations in the metabolic networks of temporal lobe epilepsy patients: a graph theoretical analysis using FDG-PET. *Neuroimage Clin* 2020; 27: 102349.
37. Yakushev I, Ripp I, Wang M, et al. Mapping covariance in brain FDG uptake to structural connectivity. *Eur J Nucl Med Mol Imaging* 2022; 49: 1288–1297.
38. Messaritaki E, Dimitriadis SI and Jones DK. Optimization of graph construction can significantly increase the power of structural brain network studies. *NeuroImage* 2019; 199: 495–511.
39. Ripp I, Emch M, Wu Q, et al. Adaptive working memory training does not produce transfer effects in cognition and neuroimaging. *Transl Psychiatry* 2022; 12: 512.
40. Rolls ET, Joliot M and Tzourio-Mazoyer N. Implementation of a new parcellation of the orbitofrontal cortex in the automated anatomical labeling atlas. *NeuroImage* 2015; 122: 1–5.
41. Avants BB, Tustison NJ, Song G, et al. A reproducible evaluation of ANTs similarity metric performance in brain image registration. *NeuroImage* 2011; 54: 2033–2044.
42. Andersson JLR and Sotiropoulos SN. An integrated approach to correction for off-resonance effects and subject movement in diffusion MR imaging. *NeuroImage* 2016; 125: 1063–1078.
43. Smith SM. Fast robust automated brain extraction. *Hum Brain Mapp* 2002; 17: 143–155.
44. Behrens TEJ, Berg HJ, Jbabdi S, et al. Probabilistic diffusion tractography with multiple fibre orientations: what can we gain? *NeuroImage* 2007; 34: 144–155.
45. van den Heuvel MP and Sporns O. Rich-club organization of the human connectome. *J Neurosci* 2011; 31: 15775–15786.
46. Bonilha L, Gleichgerrcht E, Fridriksson J, et al. Reproducibility of the structural brain connectome derived from diffusion tensor imaging (Hayasaka S, ed.). *PLoS ONE* 2015; 10: e0135247.
47. Hagmann P, Sporns O, Madan N, et al. White matter maturation reshapes structural connectivity in the late developing human brain. *Proc Natl Acad Sci U S A* 2010; 107: 19067–19072.
48. Barbagallo G, Caligiuri ME, Arabia G, et al. Structural connectivity differences in motor network between tremor-dominant and nontremor Parkinson's disease: structural network in PD phenotypes. *Hum Brain Mapp* 2017; 38: 4716–4729.
49. Nomi JS, Schettini E, Broce I, et al. Structural connections of functionally defined human insular subdivisions. *Cereb Cortex* 2018; 28: 3445–3456.
50. Buchanan CR, Bastin ME, Ritchie SJ, et al. The effect of network thresholding and weighting on structural brain networks in the UK biobank. *NeuroImage* 2020; 211: 116443.
51. Jenkinson M, Bannister P, Brady M, et al. Improved optimization for the robust and accurate linear registration and motion correction of brain images. *NeuroImage* 2002; 17: 825–841.
52. Shirer WR, Jiang H, Price CM, et al. Optimization of rs-fMRI pre-processing for enhanced signal-noise separation, test-retest reliability, and group discrimination. *NeuroImage* 2015; 117: 67–79.
53. Kalpouzos G, Chételat G, Baron JC, et al. Voxel-based mapping of brain gray matter volume and glucose metabolism profiles in normal aging. *Neurobiol Aging* 2009; 30: 112–124.
54. Wu K, Taki Y, Sato K, et al. Age-related changes in topological organization of structural brain networks in healthy individuals. *Hum Brain Mapp* 2012; 33: 552–568.
55. Tong Y, Hocke LM and Frederick BB. Low frequency systemic hemodynamic “noise” in resting state BOLD fMRI: characteristics, causes, implications, mitigation strategies, and applications. *Front Neurosci* 2019; 13: 787.
56. Geerligs L, Cam CAN and Henson RN. Functional connectivity and structural covariance between regions of interest can be measured more accurately using multivariate distance correlation. *NeuroImage* 2016; 135: 16–31.
57. Huang SY, Hsu JL, Lin KJ, et al. Characteristic patterns of inter- and intra-hemispheric metabolic connectivity in patients with stable and progressive mild cognitive impairment and Alzheimer's disease. *Sci Rep* 2018; 8: 13807.
58. Vanicek T, Hahn A, Traub-Weidinger T, et al. Insights into intrinsic brain networks based on graph theory and PET in right- compared to left-sided temporal lobe epilepsy. *Sci Rep* 2016; 6: 28513.
59. Hagmann P, Cammoun L, Gigandet X, et al. Mapping the structural core of human cerebral cortex (Friston KJ, ed.). *PLoS Biol* 2008; 6: e159.
60. Savio A, Fänger S, Tahmasian M, et al. Resting-state networks as simultaneously measured with functional MRI and PET. *J Nucl Med* 2017; 58: 1314–1317.

61. Sala A, Lizarraga A, Ripp I, et al. Static versus functional PET: making sense of metabolic connectivity. *Cereb Cortex* 2022; 32: 1125–1129.
62. Wang J, Khosrowabadi R, Ng KK, et al. Alterations in brain network topology and structural-functional connectome coupling relate to cognitive impairment. *Front Aging Neurosci* 2018; 10: 404.
63. Mechelli A, Friston KJ, Frackowiak RS, et al. Structural covariance in the human cortex. *J Neurosci* 2005; 25: 8303–8310.
64. Draganski B and May A. Training-induced structural changes in the adult human brain. *Behav Brain Res* 2008; 192: 137–142.
65. Zhao K, Zheng Q, Che T, et al. Regional radiomics similarity networks (R2SNs) in the human brain: reproducibility, small-world properties and a biological basis. *Network Neuroscience* 2021; 5: 783–797.
66. Betzel RF, Griffa A, Hagmann P, et al. Distance-dependent consensus thresholds for generating group-representative structural brain networks. *Netw Neurosci* 2019; 3: 475–496.
67. Donahue CJ, Sotiropoulos SN, Jbabdi S, et al. Using diffusion tractography to predict cortical connection strength and distance: a quantitative comparison with tracers in the monkey. *J Neurosci* 2016; 36: 6758–6770.
68. Calamante F. The seven deadly sins of measuring brain structural connectivity using diffusion MRI streamlines fibre-tracking. *Diagnostics* 2019; 69: 115.